Modal methods for the neutron diffusion equation using different spatial modes

A. Carreño[a], A. Vidal-Ferràndiz[a], D. Ginestar[b,*], G. Verdú[a]

[a] *Instituto de Seguridad Industrial, Radiofísica y Medioambiental, Universitat Politècnica de València, Camino de Vera, s/n, 46022, Valencia*
[b] *Instituto Universitario de Matemática Multidisciplinar, Universitat Politècnica de València, Camino de Vera, s/n, 46022, Valencia*

Abstract

The behaviour of the neutrons inside a nuclear reactor core can be modelled by using the time dependent neutron diffusion equation. Different time schemes have been used to integrate this equation. One possibility is to use a modal method, which is based on the expansion of the neutron flux in terms of spatial modes that are the eigenfunctions associated with a given configuration of the reactor core. Several spatial modes can be defined for the neutron diffusion equation such as the λ, α and γ-modes. In this work, the λ, the α and the γ-modes have been used to develop different modal kinetics equations, using a high order finite element method for the spatial discretization of the neutron diffusion equation. The performance of the different modal kinetic equations has been tested and compared using two 3D transient benchmark problems.

Keywords: Modal Method, Finite Element Method, Time Dependent Neutron Diffusion Equation, Spatial Modes

1. Introduction

Neutron kinetics of a nuclear power reactor can be studied by solving the time-dependent multigroup neutron diffusion equation (Stacey, 2007). In the theory and practice of neutronic calculations, fast methods have been developed to obtain accurate approximations. Some of these methods are based on the factorization of the space and time dependence of the neutronic flux (factorization methods) as, for example, the quasistatic method (Henry, 1958; Dulla et al., 2008; Yamamoto et al., 2010). These methodologies express the solution as a product of two functions: one time-dependent function (amplitude factor) and a second one that describes the spatial distribution (shape function) that can have a slow variation with time. In the point reactor approximation, the dominant

*Corresponding author
Email addresses: amcarsan@iqn.upv.es (A. Carreño), anvifer2@upv.es (A. Vidal-Ferràndiz), dginesta@mat.upv.es (D. Ginestar), gverdu@iqn.upv.es (G. Verdú)

eigenfunction associated with an auxiliar eigenvalue problem corresponding to a static configuration of the core is taken as the shape function (Akcasuh, 1971). For the quasistatic approximation, this shape function is updated over time. However, this expansion has limitations when the spatial distribution of the neutron flux changes along the transient and cannot be described using only one shape function. This occurs, for instance, in the out-of-phase oscillations observed in Boiling Water Reactors (BWR) (March-Leuba & Blakeman, 1991; March-Leuba & Rey, 1993). The generalization of this approach is the modal method (Stacey, 1969; Miró et al., 2002; de Lima et al., 2009; Avvakumov et al., 2017a) that expands the time-dependent flux as a sum of several spatial eigenfunctions of the initial configuration of the reactor. These spatial modes can be also updated along the transient (Miró et al., 2002). However, most of the time-dependent core simulators do not rely on such approximations that come from factorization methods (in spite of being, in some occasions, much more efficient in terms of the CPU time and the computational memory).

Different spectral problems can be associated with the neutron diffusion equation (Velarde et al., 1978; Ronen et al., 1976; Avvakumov et al., 2017b). The λ-modes, obtained by dividing the fission terms by a positive number, λ, have been efficiently computed (Verdú et al., 1994; Vidal-Ferrandiz et al., 2014). Other spatial modes are the α-modes, very useful to develop monitoring techniques for subcritical systems (Lewins, 2013). They are defined assuming an exponential time behavior for the neutron flux. Fast methods have been applied to obtain these modes associated with the neutron diffusion equation (Modak & Gupta, 2007; Verdu et al., 2010; Singh et al., 2011; Carreño et al., 2017). The γ-modes were presented in (Ronen et al., 1976) and appear when we make a balance between the leakage and the extraction terms and the scattering and fission terms. Recently, several techniques have been proposed for their computation in (Carreño et al., 2017). Moreover, Avvakumov et al. in (Avvakumov et al., 2017b) have formulated a new spectral problem, the δ-modes, which is connected to the self-adjoint part of operator representing neutron absorption-generation to make an a priori estimate of neutron flux dynamics. Finally, de Lima et al. (de Lima et al., 2009) have proposed to use the pseudo-harmonics that are the eigenfunctions associated with the leakage and removal operator of each energy group, which are the solutions of a self-adjoint eigenvalue problem.

The spatial modes have been successfully used in many studies to develop modal methods, mainly the λ-modes. The nodal modal kinetics associated with the λ-modes was studied in detail in (Verdú et al., 1998; Miró et al., 2002) to solve the time-dependent neutron diffusion equation and to classify instabilities in BWRs. This methodology has been also applied using a finite volume method for the spatial discretization (Bernal et al., 2016). Lange et al. in (Lange et al., 2014) used the subcritical λ-modes to study the BWR stability states. The α-modes have been also applied to study reactor instabilities (Verdú & Ginestar, 2014). More recently, the State Change Modal (SCM) method has been proposed (Avvakumov et al., 2018) based also on the calculation of the dominant α-modes. Dulla et al. in (Dulla et al., 2018) developed a fully analytical study of the spectrum of the neutron diffusion operator to analyze

some general properties of the neutron evolution.

The aim of this paper is to develop modal kinetics equations relying on the λ, the α and the γ-modes obtained using a finite element spatial discretization of the multi-group neutron diffusion equation and to compare its performance for the simulation of different transients. These modal methods make use of the dominant solutions of spectral problems associated with the neutron diffusion equation in an almost critical configuration of the reactor and can be useful to study transients in the reactor working in this configuration.

The structure of the rest of the paper is as follows. In Section 2, the time dependent neutron diffusion equation as well as the λ, γ and α-modes problems are defined in the approximation of two energy groups. Moreover, this Section includes: a brief description of the spatial discretization used for the differential equations, the definition of the adjoint problems associated to the different mode problems and the guidelines used for the computation of the spatial modes problems. In Section 3, the development of the modal kinetics equations associated with the different spatial modes is given. Numerical results to test and to compare the performance of the different modal equations for two different benchmark problems are presented in Section 4. Finally, Section 5 synthesizes the main conclusions of this work.

2. Time-dependent neutron diffusion equation

The time dependent neutron diffusion equation in the approximation of two energy groups without up-scattering and K groups of delayed neutron precursors is of the form (Stacey, 2007)

$$\begin{aligned} &\mathcal{V}^{-1}\frac{\partial \Phi}{\partial t}(\vec{r},t) + (\mathcal{L}+\mathcal{S})\Phi(\vec{r},t) = (1-\beta)\mathcal{F}\Phi(\vec{r},t) + \sum_{k=1}^{K}\lambda_k^d \mathcal{C}_k(\vec{r},t)\chi, \\ &\frac{\mathrm{d}\mathcal{C}_k}{\mathrm{d}t}(\vec{r},t) = \beta_k \mathcal{F}_1\Phi(\vec{r},t) - \lambda_k^d\mathcal{C}_k(\vec{r},t), \qquad k=1,\ldots,K, \end{aligned} \tag{1}$$

where,

$$\begin{aligned} &\mathcal{L} = \begin{pmatrix} -\vec{\nabla}\cdot(D_1\vec{\nabla}) + \Sigma_{a_1} + \Sigma_{12} & 0 \\ 0 & -\vec{\nabla}\cdot(D_2\vec{\nabla}) + \Sigma_{a_2} \end{pmatrix}, \\ &\mathcal{S} = \begin{pmatrix} 0 & 0 \\ -\Sigma_{12} & 0 \end{pmatrix}, \qquad \mathcal{F} = \begin{pmatrix} \nu\Sigma_{f_1} & \nu\Sigma_{f_2} \\ 0 & 0 \end{pmatrix}, \qquad \mathcal{F}_1 = \begin{pmatrix} \nu\Sigma_{f_1} & \nu\Sigma_{f_2} \end{pmatrix}, \\ &\mathcal{V}^{-1} = \begin{pmatrix} v_1^{-1} & 0 \\ 0 & v_2^{-1} \end{pmatrix}, \qquad \chi = \begin{pmatrix} 1 \\ 0 \end{pmatrix}, \qquad \Phi = \begin{pmatrix} \Phi_1 \\ \Phi_2 \end{pmatrix}. \end{aligned} \tag{2}$$

The diffusion coefficients (D_1,D_2), the absorption cross sections (Σ_{a1},Σ_{a2}), the scattering cross section from group 1 to group 2 (Σ_{12}) and the average number of neutrons produced in each fission multiplied by the fission cross sections ($\nu\Sigma_{f1}$, $\nu\Sigma_{f2}$) are, in general, time and position dependent functions.

Given a configuration of the reactor the criticality can be forced of several forms transforming the Equation (1) into several time-independent eigenvalue problems: the λ-modes and the γ-modes problems. The α-modes can be obtained assuming and exponential behavior for the time dependence of the neutron flux.

In this way, if the fission operator is divided by a positive number, λ_n, the λ-modes equation is obtained

$$(\mathcal{L} + \mathcal{S})\psi_n = \frac{1}{\lambda_n}\mathcal{F}\psi_n. \tag{3}$$

Secondly, if the fission and scattering terms of (1) are divided by $\gamma_n > 0$, we obtain the γ-modes problem

$$\mathcal{L}\phi_n = \frac{1}{\gamma_n}(\mathcal{F} - \mathcal{S})\phi_n. \tag{4}$$

Finally, to obtain the intermediate α-modes, that in this paper we simply denote by α-modes, we consider again the neutron diffusion equation (1) where the delayed neutron precursors are assumed to be in steady state. These modes are defined by assuming that the neutron flux admits a factorization

$$\Phi(\vec{r}, t) = e^{\alpha t}\varphi(\vec{r}), \tag{5}$$

to obtain the α-modes equation

$$(\mathcal{F} - (\mathcal{L} + \mathcal{S}))\varphi_n = \alpha_n \mathcal{V}^{-1}\varphi_n. \tag{6}$$

Other α-modes can be defined depending on different assumptions made for the neutron precursors (Verdu et al., 2010).

2.1. Finite element discretization

All of these differential equations need to be discretized to obtain an approximate solution. This spatial discretization has been done using a high order finite element discretization (for more details, see (Vidal-Ferrandiz et al., 2014)). It has been implemented by using the open source finite elements library Deal.II (Bangerth et al. (2007)). Thus, Equations (1) can be approximated by solving the system of ODE's

$$\begin{aligned} V^{-1}\frac{\mathrm{d}\tilde{\Phi}}{\mathrm{d}t} + (L+S)\tilde{\Phi} &= (1-\beta)F\tilde{\Phi} + \sum_{k=1}^{K}\lambda_k^d X C_k, \\ \frac{\mathrm{d}XC_k}{\mathrm{d}t} &= \beta_k F\tilde{\Phi} - \lambda_k^d X C_k, \qquad k = 1, \ldots, K, \end{aligned} \tag{7}$$

where L, S, F are the matrices obtained from the discretization of operators $\mathcal{L}$, $\mathcal{S}$, $\mathcal{F}$, respectively. Vectors $\tilde{\Phi}$ and C_k are the corresponding coefficients of Φ

and $\mathcal{C}_k$ in terms of the Lagrange polynomials, which are the polynomials used in the finite element method. The matrices X and $\left[V^{-1}\right]$ are defined as

$$X = \begin{pmatrix} P \\ 0 \end{pmatrix}, \qquad V^{-1} = \begin{pmatrix} Pv_1^{-1} & 0 \\ 0 & Pv_2^{-1} \end{pmatrix},$$

where P is the mass matrix of the spatial discretization, which is different from the identity matrix because the polynomial basis used in the finite element method is not orthonormal.

For spatial modes problems (Equations (3), (4), (6)), the algebraic problems associated after the discretization have, respectively, the following structure,

$$(L+S)\tilde{\psi_m} = \frac{1}{\lambda_m} F\tilde{\psi_m}, \tag{8}$$

$$L\tilde{\phi_m} = \frac{1}{\gamma_m}(F-S)\tilde{\phi_m}, \tag{9}$$

$$(F-(L+S))\tilde{\varphi_m} = \alpha_m V^{-1}\tilde{\varphi_m}, \tag{10}$$

where $\tilde{\psi}$, $\tilde{\phi}$ and $\tilde{\varphi}$ are the algebraic vectors of weights associated with the function vectors ψ, ϕ and φ, respectively. In the following, to simplify the notation, the algebraic vectors are denoted by Φ, ψ, ϕ and φ by removing the tildes from the original notation.

2.2. Adjoint spectral problems

Associated to each spatial problem, we can introduce an adjoint problem (Henry, 1982). For the λ-modes problem, we define the adjoint problem as

$$(L+S)^{\mathsf{T}}\psi_l^\dagger = \frac{1}{\lambda_l} F^{\mathsf{T}}\psi_l^\dagger, \tag{11}$$

where L^{T}, S^{T} and F^{T} are the transpose matrices of L, S and F, respectively, that are equal to the matrices obtained from the discretization of the adjoint operators, $\mathcal{L}^\dagger$, $\mathcal{S}^\dagger$ and $\mathcal{F}^\dagger$. The adjoint modes obtained, $\psi_l^\dagger$, $l = 1, \ldots, q$ satisfy the biorthogonality condition

$$\langle \psi_l^\dagger, F\psi_m \rangle = \langle \psi_m^\dagger, F\psi_m \rangle \delta_{l,m}, \quad l, m = 1, \ldots, q, \tag{12}$$

where $\langle\,,\rangle$ is the scalar product for vectors and $\delta_{l,m}$ is the Kronecker's delta.

Likewise, we define the adjoint problem for the γ-modes

$$L^{\mathsf{T}}\phi_l^\dagger = \frac{1}{\gamma_l}(F^{\mathsf{T}} - S^{\mathsf{T}})\phi_l^\dagger. \tag{13}$$

In this case, the adjoint γ-modes, $\phi_l^\dagger$, $\quad l = 1, \ldots, q$, satisfy the biorthogonality condition

$$\langle \phi_l^\dagger, (F-S)\phi_m \rangle = \langle \phi_m^\dagger, (F-S)\phi_m \rangle \delta_{l,m}, \quad l, m = 1, \ldots, q. \tag{14}$$

Lastly, for the α-modes, we introduce the adjoint problem

$$(F^{\mathsf{T}} - (L^{\mathsf{T}} + S^{\mathsf{T}}))\varphi_l^{\dagger} = \alpha_l V^{-1}\varphi_l^{\dagger}. \tag{15}$$

Note that, the symmetry of the V^{-1} operator implies that $V^{-1,\mathsf{T}} = V^{-1}$.

Therefore, the adjoint α-modes $\varphi_l^{\dagger}$, $l = 1, \ldots, q$ satisfy the biorthogonality condition

$$\langle \varphi_l^{\dagger}, V^{-1}\varphi_m \rangle = \langle \varphi_m^{\dagger}, V^{-1}\varphi_m \rangle \delta_{l,m}, \quad l, m = 1, \ldots, q. \tag{16}$$

2.3. Eigenvalue computations

The dominant solutions for the problems associated with the spatial modes (8), (9) and (10) have been obtained by using the strategy presented in (Carreño et al., 2017). In this work, the λ-modes are computed with the Krylov-Schur method implemented in the SLEPc library (Hernandez et al., 2005) by reformulating this problem as an ordinary eigenvalue problem. As the matrices L, S and F can be expressed with the following block structure for two energy groups

$$L = \begin{pmatrix} L_{11} & 0 \\ 0 & L_{22} \end{pmatrix}, \quad S = \begin{pmatrix} 0 & 0 \\ S_{21} & 0 \end{pmatrix} \quad \text{and } F = \begin{pmatrix} F_{11} & F_{12} \\ 0 & 0 \end{pmatrix},$$

the generalized λ-modes problem (8) can be reformulated as an ordinary eigenvalue problem

$$L_{11}^{-1}(F_{11} - F_{12}L_{22}^{-1}S_{21})\psi_{m,1} = \lambda_m \psi_{m,1}$$

where the product of the inverse blocks by a vector is computed by means of solving linear systems. The vector $\psi_{m,1}$ corresponds to the fast flux of the m-th mode. The thermal flux, $\psi_{m,2}$ is computed from the approximation $\psi_{m,1}$. The computation of the other spatial modes is carried out with the modified block Newton method for generalized eigenvalue problems based on the Rayleigh-Ritz algorithm (MGBNM). It has been shown in other works that the computation of the α and γ-modes is more expensive than the computation of the λ-modes. Thus, we use an initialization strategy from the solution of the λ-modes problem, by applying a Rayleigh-Ritz procedure, to obtain an initial guess for the MGBNM. Thus, if U^{λ} is the matrix whose columns are the eigenfunctions obtained from the λ-modes problem, we compute the initial approximation from the Ritz vectors of the problem projected over U^{λ}. For the γ-modes problem, we solve the problem

$$U^{\lambda}LU^{\lambda}Z^{\gamma} = \frac{1}{\gamma_m}U^{\lambda}(F - S)U^{\lambda}Z^{\gamma},$$

and then, the approximate eigenvectors are obtained from $U^{\gamma} = U^{\lambda}Z^{\gamma}$. For the α-modes case, we need to solve the problem

$$U^{\lambda}(F - (L + S))U^{\lambda}Z^{\alpha} = \alpha_m U^{\lambda}V^{-1}U^{\lambda}Z^{\alpha},$$

and then the approximate eigenvectors are given by $U^{\alpha} = U^{\lambda} Z^{\alpha}$. The adjoint modes are computed from the direct modes following a similar strategy as the strategy applied for the γ and α-modes. In this case, we apply once the Rayleigh-Ritz process by projecting over the eigenvectors associated with direct problems and then a fixed point method is used to converge the adjoint modes.

For reactors without spatial symmetry, the eigenvalues solution of problems (11), (13) and (15) are not degenerated and the adjoint eigenvectors computed are biorthogonal, thus we only need to divide each adjoint vector $\psi_l^{\dagger}$, $\phi_l^{\dagger}$, $\varphi_l^{\dagger}$ by the product $\langle {\psi_l}^{\dagger}, F\psi_l \rangle$, $\langle {\psi_l}^{\dagger}, (F-S)\psi_l \rangle$ and $\langle {\psi_l}^{\dagger}, V^{-1}\psi_l \rangle$, respectively, to obtain a biorthonormal basis. For reactors with radial symmetry, it can be proved (see (Tommasi et al., 2016)) that degenerated eigenvalues (i.e. eigenvalues with multiplicity greater than 1) can appear and consequently the adjoint modes computed are not directly biorthogonal. This problem is solved by using the biorthogonalization procedure shown in Algorithm 1 (Adrover et al., 2005).

Algorithm 1 Biorthogonalization process

Input: The adjoint eigenvectors $\hat{V} = [\hat{V_1}, \ldots, \hat{V_q}]$, the direct eigenvectors $\hat{Z} = [\hat{Z_1}, \ldots, \hat{Z_q}]$.
Output: $V = [V_1, \ldots, V_q]$, $Z = [Z_1, \ldots, Z_q]$ such that $V^{\mathsf{T}} A Z = I_q$.

```
V = V̂, Z = Ẑ
for k = 0 to k < q do
    V_k = V_k/(V_k^T A Z_k)
    for i = k + 1 to i < q do
        Z_i = Z_i − (V_k^T A Z_i) Z_k
        V_i = V_i − (V_i^T A Z_k) V_k
    end for
end for
```

3. Modal kinetics

To solve the time-dependent neutron diffusion equation (7) by using a modal method, we suppose that $\Phi(\vec{r}, t)$ admits the following expansion

$$\Phi(\vec{r}, t) = \sum_{m=1}^{q} n_m^{\delta}(t) \xi_m(\vec{r}), \tag{17}$$

where $\xi_m(\vec{r})$ are the unitary eigenvectors associated with the m-th dominant eigenvalues of some static problem (8), (9) or (10) and q is the number of dominant modes considered. The amplitude coefficients $n_m^{\delta}(t)$ are only time dependent and they will change with the kind of spatial mode used ($\delta = \lambda, \gamma, \alpha$). To simplify the notation, we will write n_m and ψ_m instead of $n_m(t)$ and $\psi_m(\vec{r})$.

For each kind of modes problem, we choose the matrices L, S and F, that we denote by L_0, S_0 and F_0, as the matrices related to the configuration of the reactor core at $t = 0$. We start with this reactor in critical state by dividing

the matrix related to the fission terms (F_0) by $k_{eff} = \lambda_1$. However, note that if we force the transient to start the computation with the reactor in critical state, the dominant α-mode will be equal to zero and the numerical methods have some convergence problems. So, in the case of the α-modes, we divide the fission cross-section by $k_{eff} + 10^{-8}$ obtaining a reactor quasi critical. In this way, we express the matrices L and F as

$$L = L_0 + \delta L, \qquad S = S_0, \qquad F = F_0 + \delta F. \tag{18}$$

If we use the expansion (17) until a certain number of modes, q, the equations (7) are equivalent to

$$\begin{aligned} &V^{-1} \sum_{m=1}^{q} \frac{\mathrm{d}n_m^\delta}{\mathrm{d}t}\xi_m + \sum_{m=1}^{q} L_0 n_m^\delta \xi_m + \sum_{m=1}^{q} \delta L n_m^\delta \xi_m + \sum_{m=1}^{q} S_0 n_m^\delta \xi_m \\ &= (1-\beta)\sum_{m=1}^{q} F_0 n_m^\delta \xi_m + (1-\beta)\sum_{m=1}^{q} \delta F n_m^\delta \xi_m + \sum_{k=1}^{K} \lambda_k^d X C_k, \\ &\frac{\mathrm{d}XC_k}{\mathrm{d}t} = \sum_{m=1}^{q} \beta_k F_0 n_m^\delta \xi_m + \sum_{m=1}^{q} \beta_k \delta F n_m^\delta \xi_m - \lambda_k^d X C_k, \qquad k = 1, \ldots, K. \end{aligned} \tag{19}$$

Hereafter, we particularize the equations obtained for each kind of spatial mode. By using the dominant λ-modes, Equation (19) can be rewritten as

$$\begin{aligned} &V^{-1} \sum_{m=1}^{q} \frac{\mathrm{d}n_m^\lambda}{\mathrm{d}t}\psi_m + \sum_{m=1}^{q} \frac{1}{\lambda_m} F_0 n_m^\lambda \psi_m + \sum_{m=1}^{q} \delta L n_m^\lambda \psi_m \\ &= (1-\beta)\sum_{m=1}^{q} F_0 n_m^\lambda \psi_m + (1-\beta)\sum_{m=1}^{q} \delta F n_m^\lambda \psi_m + \sum_{k=1}^{K} \lambda_k^d X C_k, \\ &\frac{\mathrm{d}XC_k}{\mathrm{d}t} = \sum_{m=1}^{q} \beta_k F_0 n_m^\lambda \psi_m + \sum_{m=1}^{q} \beta_k \delta F n_m^\lambda \psi_m - \lambda_k^d X C_k, \qquad k = 1, \ldots, K. \end{aligned} \tag{20}$$

Then, Equations (20) are multiplied by the adjoint modes $\psi_l^\dagger$ with $l = 1, \ldots, q$ and the biorthogonality condition (12) is used to obtain the following system of $q(K+1)$ equations

$$\begin{cases} \displaystyle\sum_{m=1}^{q} \langle \psi_l^\dagger, V^{-1}\psi_m \rangle \frac{\mathrm{d}}{\mathrm{d}t} n_m^\lambda + \frac{1}{\lambda_l} n_l^\lambda + \sum_{m=1}^{q} \langle \psi_l^\dagger, \delta L \psi_m \rangle n_m^\lambda = (1-\beta) n_l \\ \displaystyle +(1-\beta)\sum_{m=1}^{q} \langle \psi_l^\dagger, \delta F \psi_m \rangle n_m^\lambda + \sum_{k=1}^{K} \lambda_k^d \langle \psi_l^\dagger, X C_k \rangle, \qquad l = 1, \ldots, q, \\ \\ \displaystyle\frac{\mathrm{d}}{\mathrm{d}t}\langle \psi_l^\dagger, X C_k \rangle = \beta_k n_l^\lambda + \beta_k \textstyle\sum_{m=1}^{q} \langle \psi_l^\dagger, \delta F \psi_m \rangle n_m^\lambda \\ \qquad\qquad\qquad\qquad -\lambda_k^d \langle \psi_l^\dagger, X C_k \rangle, \quad k = 1, \ldots, K. \end{cases} \tag{21}$$

Reordering terms and introducing the notation

$$\begin{aligned} &\Lambda^{\lambda}_{lm} = \langle \psi^{\dagger}_l, V^{-1}\psi_m \rangle, \quad \Delta L^{\lambda}_{lm} = \langle \psi^{\dagger}_l, \delta L \psi_m \rangle, \\ &\Delta F^{\lambda}_{lm} = \langle \psi^{\dagger}_l, \delta F \psi_m \rangle, \quad c^{\lambda}_{lk} = \langle \psi^{\dagger}_l, X C_k \rangle, \end{aligned} \tag{22}$$

the system of equations (21) can be expressed as

$$\begin{cases} \displaystyle\sum_{m=1}^{q} \Lambda^{\lambda}_{lm} \frac{\mathrm{d}}{\mathrm{d}t} n^{\lambda}_m = & (1 - \dfrac{1}{\lambda_l} - \beta) n^{\lambda}_l - \sum_{m=1}^{q} \Delta L^{\lambda}_{lm} n^{\lambda}_m \\ & + (1-\beta) \sum_{m=1}^{q} \Delta F^{\lambda}_{lm} n^{\lambda}_m + \sum_{k=1}^{K} \lambda^d_k c^{\lambda}_{lk}, \qquad l = 1, \ldots, q. \\ \dfrac{\mathrm{d}}{\mathrm{d}t} c^{\lambda}_{lk} = \beta_k n^{\lambda}_l + \beta_k \displaystyle\sum_{m=1}^{q} \Delta F^{\lambda}_{lm} n^{\lambda}_m - \lambda^d_k c^{\lambda}_{lk}, \qquad k = 1, \ldots, K, \end{cases} \tag{23}$$

In matrix form, the system (23) can be also expressed as

$$\frac{\mathrm{d}}{\mathrm{d}t} \mathbf{N}^{\lambda} = \mathbf{T}^{\lambda} \mathbf{N}^{\lambda}, \tag{24}$$

where

$$\mathbf{N}^{\lambda} = \begin{pmatrix} n^{\lambda}_1 \cdots n^{\lambda}_q & c^{\lambda}_{11} \cdots c^{\lambda}_{q1} & \cdots & c^{\lambda}_{1K} \cdots c^{\lambda}_{qK} \end{pmatrix}^{\mathsf{T}} \tag{25}$$

and

$$\mathbf{T}^{\lambda} = \left(\begin{array}{c|ccc} \Lambda^{-1}_{\lambda}((1-\beta)I - [\lambda]^{-1} - \Delta L^{\lambda} + (1-\beta)\Delta F^{\lambda}) & \Lambda^{-1}_{\lambda}\lambda^d_1 & \cdots & \Lambda^{-1}_{\lambda}\lambda^d_K \\ \hline \beta_1(I + \Delta F^{\lambda}) & -\lambda^d_1 I & \cdots & 0 \\ \vdots & \vdots & \ddots & \vdots \\ \beta_K(I + \Delta F^{\lambda}) & 0 & \cdots & -\lambda^d_K I \end{array} \right). \tag{26}$$

The block $[\lambda]$ denotes the diagonal matrix whose elements are the dominant λ eigenvalues and I is the identity matrix.

Through an analogous process for the γ and α-modes, we obtain similar differential systems. For the γ-modes, by using their corresponding biorthogonality condition, the following matrix system is obtained

$$\frac{\mathrm{d}}{\mathrm{d}t} \mathbf{N}^{\gamma} = \mathbf{T}^{\gamma} \mathbf{N}^{\gamma}, \tag{27}$$

where

$$\mathbf{N}^{\gamma} = \begin{pmatrix} n^{\gamma}_1 \cdots n^{\gamma}_q & c^{\gamma}_{11} \cdots c^{\gamma}_{q1} & \cdots & c_{1K} \cdots c^{\gamma}_{qK} \end{pmatrix}^{\mathsf{T}}, \tag{28}$$

$$\mathbf{T}^{\gamma} = \left(\begin{array}{c|ccc} \Lambda^{-1}_{\gamma}(I - [\gamma]^{-1} - \Delta L^{\gamma} - \beta A^{F,\gamma} + (1-\beta)\Delta F^{\gamma}) & \Lambda^{-1}_{\gamma}\lambda^d_1 & \cdots & \Lambda^{-1}_{\gamma}\lambda^d_K \\ \hline \beta_1(A^{F,\gamma} + \Delta F^{\gamma}) & -\lambda^d_1 I & \cdots & 0 \\ \vdots & \vdots & \ddots & \vdots \\ \beta_K(A^{F,\gamma} + \Delta F^{\gamma}) & 0 & \cdots & -\lambda^d_K I \end{array} \right), \tag{29}$$

and

$$\begin{aligned} A^{F,\gamma}_{lm} &= \langle \phi^\dagger_l, F_0\phi_m\rangle, & \Delta L^{\gamma}_{lm} &= \langle \phi^\dagger_l, \delta L\phi_m\rangle, \\ \Delta F^{\gamma}_{lm} &= \langle \phi^\dagger_l, \delta F\phi_m\rangle, & c^{\gamma}_{lk} &= \langle \phi^\dagger_l, XC_k\rangle, \\ \Lambda^{\gamma}_{lm} &= \langle \phi^\dagger_l, \left[v^{-1}\right]\phi_m\rangle, \end{aligned} \tag{30}$$

The block $[\gamma]$ denotes the diagonal matrix whose elements are the dominant values of γ.

If now, we use the α-modes problem and its associated adjoint problem, we have the following system

$$\frac{\mathrm{d}}{\mathrm{d}t}\mathbf{N}^\alpha = \mathbf{T}^\alpha\mathbf{N}^\alpha, \tag{31}$$

where

$$\mathbf{N}^\alpha = \begin{pmatrix} n^\alpha_1 \cdots n^\alpha_q & c^\alpha_{11}\cdots c^\alpha_{q1} & \cdots & c^\alpha_{1K}\cdots c^\alpha_{qK}\end{pmatrix}^{\mathsf{T}}, \tag{32}$$

$$\mathbf{T}^\alpha = \left(\begin{array}{c|ccc} ([\alpha] - \beta A^{F,\alpha} - \Delta L^\alpha + (1-\beta)\Delta F^\alpha) & \lambda^d_1 & \cdots & \lambda^d_K \\ \hline \beta_1(A^{F,\alpha} + \Delta F^\alpha) & -\lambda^d_1 I & \cdots & 0 \\ \vdots & \vdots & \ddots & \vdots \\ \beta_K(A^{F,\alpha} + \Delta F^\alpha) & 0 & \cdots & -\lambda^d_K I \end{array}\right) \tag{33}$$

and

$$\begin{aligned} A^{F,\alpha}_{lm} &= \langle \varphi^\dagger_l, F_0\varphi_m\rangle, & \Delta L^{\alpha}_{lm} &= \langle \varphi^\dagger_l, \delta L\varphi_m\rangle, \\ \Delta F^{\alpha}_{lm} &= \langle \varphi^\dagger_l, \delta F\varphi_m\rangle, & c^{\alpha}_{lk} &= \langle \varphi^\dagger_l, XC_k\rangle. \end{aligned} \tag{34}$$

The block $[\alpha]$ denotes the diagonal matrix whose elements are the dominant values of α.

All systems of differential equations need initial conditions to be solved. From the equations in the steady state, these conditions are

$$\begin{aligned} n^\delta_1(0) &= 1, & n^\lambda_m(0) &= 0,\ m = 2,\ldots,q \\ c^\delta_{1k}(0) &= \frac{\beta_k}{\lambda^d_k}\langle \xi^\dagger_1, F_0\xi_1\rangle, & c^\delta_{mk}(0) &= 0,\ m = 2,\ldots,q, \quad k = 1,\ldots,K, \end{aligned}$$

with ξ_1 and $\xi^\dagger_1$, $\xi = \phi, \psi, \varphi$ the corresponding eigenvector and its adjoint of the dominant eigenvalue $\delta = \lambda, \gamma, \alpha$.

The system of differential equations obtained for the different spatial modes is quite smaller than the original system (7) when the number of eigenvalues used in the expansion, q, is not too large. These systems are stiff, so implicit methods are needed to obtain approximate solutions. In this work, we use a backward differentiation formula implemented in the CVODE solver from the SUNDIALS library (Hindmarsh et al., 2005; Abhyankar et al., 2018). This code has implemented an adaptive time step and it is initialized with time step of 10^{-3}s.

4. Numerical results

In this Section, we present numerical results obtained for two three-dimensional benchmarks to compare the performance of the different modal methods presented above. The first benchmark is a theoretical transient that has been used to validate the code. The second one is a more realistic benchmark, the Langenbuch reactor (Langenbuch et al., 1977), that has been perturbed with an out-of-phase local oscillation in the material cross sections. For each reactor, the results obtained with the modal methods have been compared with the ones obtained with a code that integrates Equation (7) by using a temporal discretization based on the one-step backward difference formula and a finite element spatial discretization (Ginestar et al., 1998; Vidal-Ferràndiz et al., 2016). We denote this method by BKM and take its results as reference.

All results are computed using a degree of the polynomial equal to 3 in the the finite element method, since it has been shown in other works that this degree is enough to obtain accurate results for usual reactor calculations (Vidal-Ferrandiz et al., 2014).

In this work, we have computed the relative errors related to the neutron power that we describe hereafter. The neutron Power (P) is defined as

$$\mathrm{P}^{\delta}(\vec{r},t) = \Sigma_{f,1}\xi_1(\vec{r},t) + \Sigma_{f,2}\xi_2(\vec{r},t),$$

where $\delta = \lambda, \gamma, \alpha$ is the eigenvalue associated to the eigenvector $\xi = \psi, \phi, \varphi$, respectively. In the steady state computations, we normalized the fluxes taking the mean power equal to 1, i.e,

$$1 = \frac{1}{V}\int_{\Omega} \mathrm{P}^{\delta}(\vec{r},t)\mathrm{d}\vec{V},$$

where V denotes the total volume of the reactor and Ω the reactor domain.

The Power Error (PE) in the cell (i,j,k) is given by

$$\mathrm{PE}^{\delta}_{i,j,k}(t) = \frac{|\bar{\mathrm{P}}^{\delta}_{i,j,k}(t) - \bar{\mathrm{P}}^{\delta,\mathrm{ref}}_{i,j,k}(t)|}{|\bar{\mathrm{P}}^{\delta,\mathrm{ref}}_{i,j,k}(t)|},$$

where $\bar{\mathrm{P}}^{\delta}_{i,j,k}$ and $\bar{\mathrm{P}}^{\delta,\mathrm{ref}}_{i,j,k}$ are the obtained power and the reference power in the cell (i,j,k) (cell average), respectively.

The Mean Power Error (MPE) is defined by

$$\mathrm{MPE}^{\delta}(t) = \frac{1}{V_t}\sum_{i,j,k} \mathrm{PE}^{\delta}_{i,j,k}(t)V_{i,j,k},$$

where V_t is the total volume of the reactor core and $V_{i,j,k}$ is the volume of the cell (i,j,k).

The Radial Power Error (RPE) is defined by

$$\mathrm{RPE}^{\delta}_{i,j}(t) = \frac{1}{H}\sum_{k} \mathrm{PE}^{\delta}_{i,j,k}(t)V_{i,j,k},$$

where H is the height of the reactor core.

The modal methodology and the Backward method have been implemented in C++ based on the data structures provided by the library Deal.II (Bangerth et al., 2007) and PETSc (Balay et al., 2018). The computer used for the computations was an Intel® Core™i7-4790 3.60 GHz with 32 Gb of RAM running on Ubuntu GNU/Linux 16.04 LTS.

4.1. Cuboid reactor

This transient is based on a non homogeneous prismatic reactor. It is composed of 72 equal nodes ($3\times3\times8$) of dimension $30\times30\times30$ cm^3 whose distribution is represented in Figure 1. Table 1 collects the material cross sections. The constants associated with the the six groups of precursors are displayed in Table 2. The neutron velocities are v_1= 10^7cm/s and v_2= 10^5cm/s. The boundary conditions are zero flux. For this reactor, we have computed the five dominant λ, γ and α-modes. The results for the eigenvalues obtained are shown in Table 3.

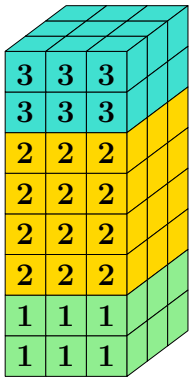

Figure 1: Distribution of the materials for the cuboid reactor.

Table 1: Material cross section for the cuboid reactor.

Mat.	Group	D_g (cm)	Σ_{ag} (cm^{-1})	$\nu\Sigma_{fg}$ (cm^{-1})	Σ_{fg} (cm^{-1})	Σ_{12} (cm^{-1})
1	1	1.695310	0.0139530	0.01340976	0.01340976	0.0164444
	2	0.409718	0.2614097	0.34239791	0.34239791	-
2	1	1.695310	0.0139954	0.01340976	0.01340976	0.0164444
	2	0.409718	0.2614200	0.34239791	0.34239791	-
3	1	1.695310	0.0139523	0.01340976	0.01340976	0.0164444
	2	0.409718	0.2614095	0.34239791	0.34239791	-

The transient analyzed has been defined from a time-dependent perturbation to the fission cross sections of the material 1 so that the neutron power increases

Table 2: Constants for the neutron precursors for the cuboid reactor.

Group	1	2	3	4	5	6
β_g	0.000247	0.0013845	0.001222	0.0026455	0.000832	0.000169
$\lambda_g(\mathrm{s}^{-1})$	0.0127	0.0317	0.115	0.311	1.4	3.87

Table 3: Five dominant modes for the cuboid reactor.

Mode	λ-modes	γ-modes	α-modes
1	1.000000	1.000000	-0.03801
2	0.975493	0.984772	-925.650
3	0.936569	0.960346	-2371.33
4	0.886212	0.928279	-4195.81
5	0.842369	0.899897	-5741.37

during 2 seconds and then it decreases. The functions that define the time evolution of the cross sections are

$$\nu\Sigma_{f1}(t) = \begin{cases} 0.01340976\big(1 + \dfrac{0.0122}{0.8}t\big), & 0 \le t \le 2, \\ 0.01381876\big(1 - \dfrac{0.0122}{0.8}(t-2)\big), & 2 \le t \le 4, \end{cases}$$

$$\nu\Sigma_{f2}(t) = \begin{cases} 0.34239791\big(1 + \dfrac{0.0122}{0.8}t\big), & 0 \le t \le 2, \\ 0.35284104\big(1 - \dfrac{0.0122}{0.8}(t-2)\big), & 2 \le t \le 4. \end{cases}$$

To study and compare the performance of the different modal methods, we have solved this problem using different number of modes. In Figure 2, the power evolution obtained for the transient using the λ, γ and α modes is represented, together with the power evolution obtained with the BKM, taken as a reference. This Figure shows that the obtained approximations improve when the number of modes used is increased, but this number of modes is not large enough to describe accurately the transient. This is due to the fact that the perturbation is applied only to the material 1 and the modes have difficulties to catch the very localized character of the response of the system. A high number of modes would be required to obtain better approximations. However, even if the modal methods cannot be the best technique to approximate this transient, this is an interesting challenging problem to test the modal methods. Moreover, a comparison of the evolution of the power obtained with the different modal methods has been included (Figure 2(d)) by using 3 eigenvalues. In this last graphic, we do not observe big differences between the kind of modes used in the expansion of the flux.

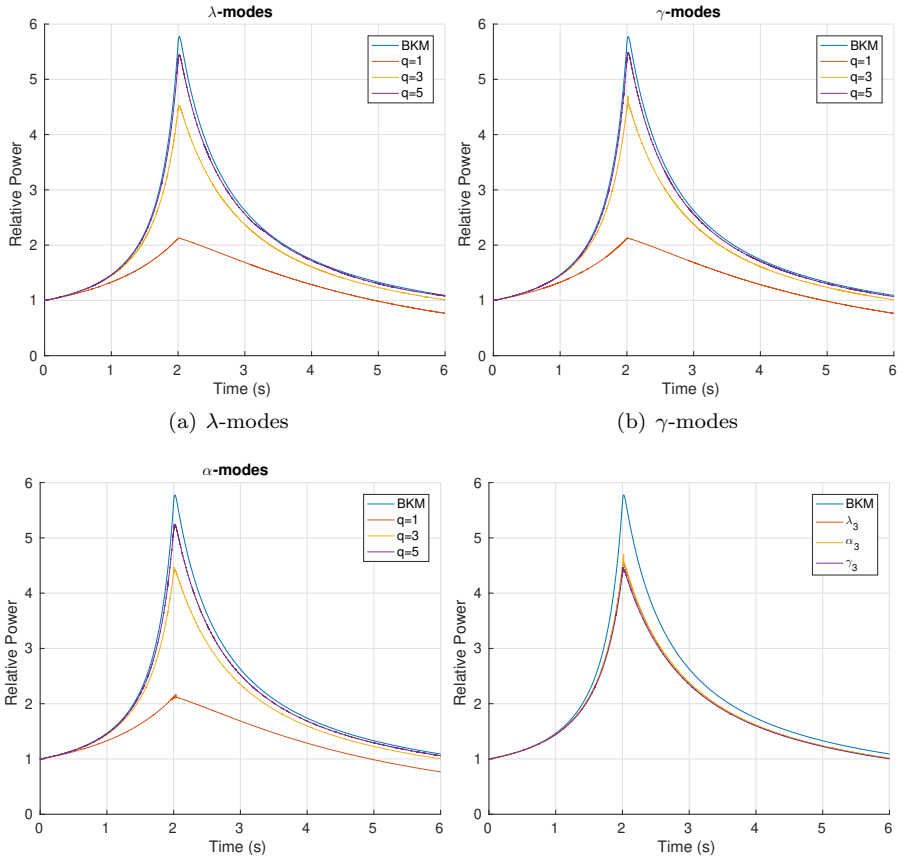

(a) λ-modes (b) γ-modes

(c) α-modes (d) λ, α, γ (3 modes)

Figure 2: Evolution of the power of the cuboid transient.

Finally, we compare the computational time (CPU time) to obtain the solution by using the BKM and the modal kinetics methods with the different spatial modes. Table 4 displays these results for several number of eigenvalues. Moreover, this Table includes the Mean Power Error (MPE) at $t = 2.0$ (taking the result obtained with the BKM as a reference) to quantify the error made by the modal approximations. First, this Table shows (as it does Figure 2) that the MPE decreases when the number of eigenvalues considered in the modal kinetics is increased. Nevertheless, the results shows that it is not computationally efficient to use a number of modes very high, since the computational time also increases when the number of eigenvalues is higher. In comparison with the BKM, one can observe that using modal methods is much more efficient than using the BKM (in spite of a high number of eigenvalues is required to obtain accurate approximations). Between the different spatial modes, the modal kinetics with the expansion of the γ-modes is the most efficient option since the

best approximations are obtained with the shortest time.

Table 4: Mean Power Error (MPE) at $t = 2.0$ and CPU times (s) to obtain the relative power of the cuboid reactor.

Method	MPE(2.0)	CPU Time (s)
BKM	-	5377
Modal Kinetics (λ)		
$q = 1$	3.52e+0	84
$q = 3$	1.19e+0	529
$q = 5$	3.21e-1	675
$q = 9$	1.19e-1	1182
$q = 12$	1.16e-1	1392
Modal Kinetics (γ)		
$q = 1$	3.52e+0	153
$q = 3$	1.15e+0	368
$q = 5$	4.35e-1	413
$q = 9$	4.41e-2	532
$q = 12$	2.83e-2	892
Modal Kinetics (α)		
$q = 1$	3.52e+0	51
$q = 3$	1.28e+0	108
$q = 5$	5.09e-1	370
$q = 9$	3.34e-1	761
$q = 12$	3.24e-1	878

4.2. Langenbuch reactor

The Langenbuch 3D benchmark (Langenbuch et al., 1977) is chosen to compare the modal schemes in a more realistic case. It has 1170 different assemblies including 545 cells modelling the reflector. The definition of the 5 different materials and their cross sections are given in Figure 3, Figure 4 and Table 5. The velocities are $v_1 = 1.25 \cdot 10^7$cm/s and $v_2 = 2.5 \cdot 10^5$cm/s. The information about the delayed precursors is in Table 2, since these values are the same as the ones used for the cuboid reactor. Boundary conditions are zero-flux. This transient has been computed without reactivity feedback.

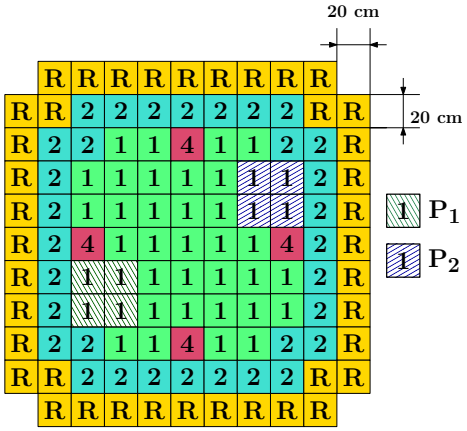

Figure 3: Top view of the Langenbuch 3D reactor.

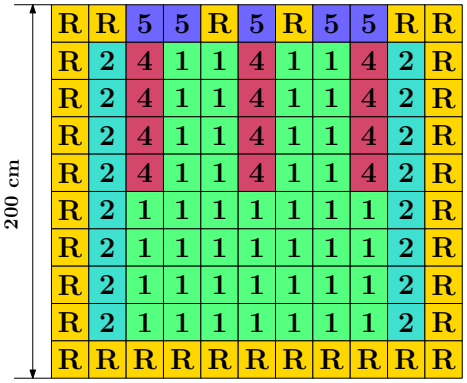

Figure 4: Lateral view of the Langenbuch 3D reactor.

Table 5: Macroscopic cross sections of the Langenbuch 3D reactor.

Mat.	Group	D_g (cm)	Σ_{ag} (cm^{-1})	$\nu\Sigma_{fg}$ (cm^{-1})	Σ_{fg} (cm^{-1})	Σ_{12} (cm^{-1})
1	1	1.423913	0.01040206	0.0064792	0.0025916	0.01755550
	2	0.3563060	0.08766217	0.1127612	0.0451044	-
2	1	1.425611	0.01099263	0.0075051	0.0030020	0.01717768
	2	0.3505740	0.09925634	0.1378351	0.0551340	-
R	1	1.634227	0.00266057	0.0000000	0.0000000	0.02759693
	2	0.2640020	0.04933510	0.0000000	0.0000000	-
4	1	1.423913	0.01095206	0.0064792	0.0025916	0.01755550
	2	0.3563060	0.09146217	0.1127612	0.0451044	-
5	1	1.634227	0.00321050	0.0000000	0.0000000	0.02759693
	2	0.2640020	0.05316351	0.0000000	0.0000000	-

The first five dominant eigenvalues associated with this reactor are displayed in Table 6. This Table shows that the reactor is critical, since we have forced to start in critical state. Note that, the first α-modes is not equal to zero, since for the calculation of these modes we have imposed that the reactor was not exactly critical. Moreover, the second and the third eigenvalue are degenerated due to the spatial symmetry of the reactor. The power harmonic modes, defined as

$$P_n = \Sigma_{f_1}\xi_{1,n} + \Sigma_{f_2}\xi_{2,n}, \text{where, } \xi = \psi, \phi, \varphi, \tag{35}$$

of the average plane $x - y$ are represented in Figure 5. The distributions of the relative power corresponding to the first eigenvalues, that represent the power of the reactor in steady state, are identical for the three kind of modes. The power distribution for the second and third modes are different. The power harmonic for the fourth mode is an axial mode. The axial profile is symmetric to the median plane and as a consequence, the average power in the plane is near zero.

Table 6: Five dominant modes for the Langenbuch reactor.

Mode	λ-modes	γ-modes	α-modes
1	1.000000	1.000000	-0.00026
2	0.968020	0.981841	-867.189
3	0.968020	0.981841	-867.189
4	0.951963	0.972668	-1277.52
5	0.937756	0.964403	-1710.17

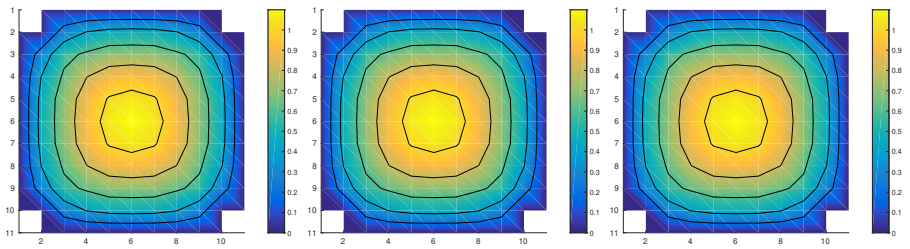

(a) λ_1 (b) γ_1 (c) α_1

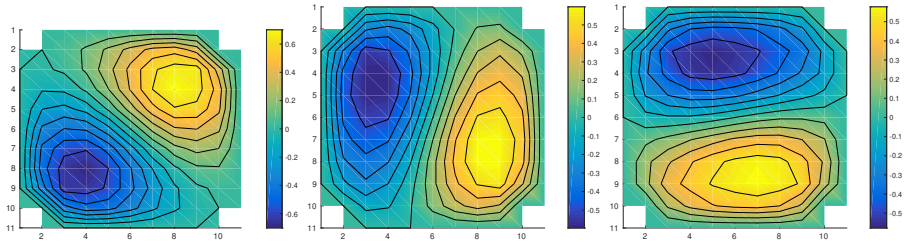

(d) λ_2 (e) γ_2 (f) α_2

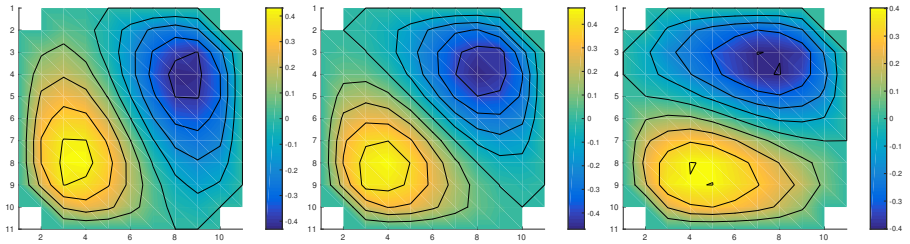

(g) λ_3 (h) γ_3 (i) α_3

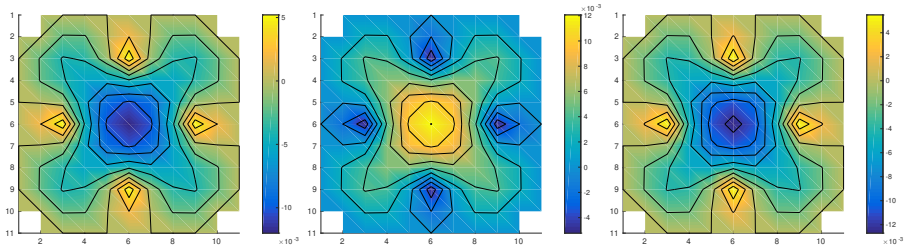

(j) λ_4 (k) γ_4 (l) α_4

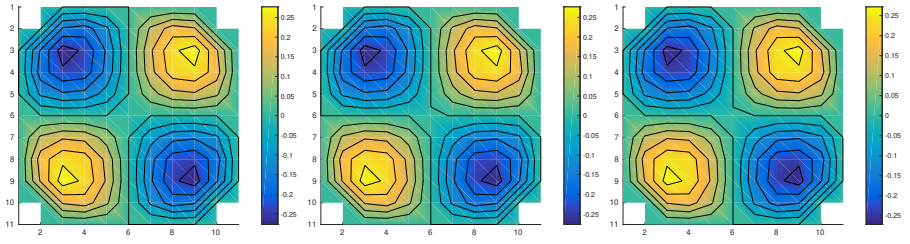

(m) λ_5 (n) γ_5 (o) α_5

Figure 5: Power in the mean plane of the Langenbuch reactor.

The transient analyzed has been defined by perturbing the fission cross sections of material 1 represented in the Figure 3 with striped pattern. We have defined two types of local sinusoidal perturbations that are out of phase between them defined as

$$\Sigma_{f,g}(t) = \Sigma_{f_0,g}(t) + \delta\Sigma_{f,g}(t) \qquad g = 1, 2. \tag{36}$$

The perturbation 1, represented in the Figure 3 as P_1, is given by

$$\delta\Sigma_{f,g}(t) = 5 \cdot 10^{-4} \sin(\omega 2\pi t) \qquad g = 1, 2,$$

and the perturbation 2, denoted by P_2, is given by

$$\delta\Sigma_{f,g}(t) = 5 \cdot 10^{-4} \sin(\omega 2\pi t + \pi) \qquad g = 1, 2,$$

where $\omega = 1.0$.

We want to highlight that the reactor is perturbed locally and this induces local changes in the spatial power distribution which makes this transient a challenging one to be solved using spatial modal methods.

First, we have computed the power evolution by using the Backward Difference method (BKM). Figure 6 represents the radial average power distribution at four relevant times ($t = 0.00$, $t = 0.25$, $t = 0.50$ and $t = 0.75$). It is observed that at first the maximum power goes from the center to the perturbation 1 zone then, it comes back to the center and then, it goes to the perturbation 2 zone. This behavior is repeated along the transient.

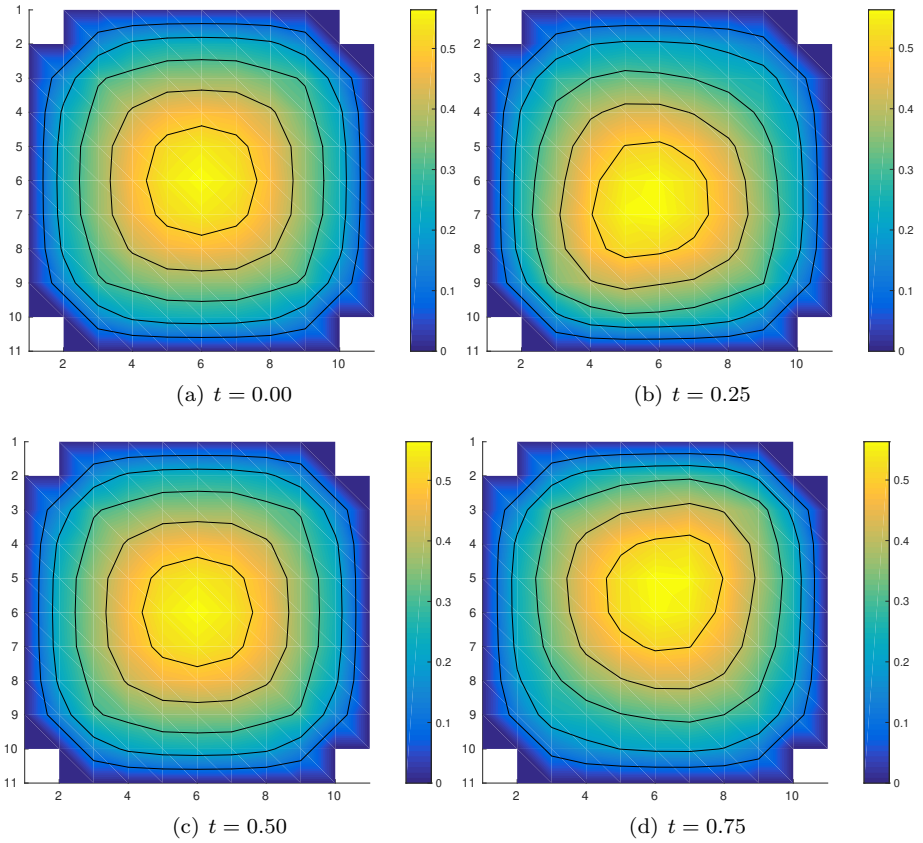

(a) $t = 0.00$ (b) $t = 0.25$

(c) $t = 0.50$ (d) $t = 0.75$

Figure 6: Evolution power of the Langenbuch transient at $t = 0.00, t = 0.25, 0.50, 0.75$ with three eigenvalues.

We have computed the time dependent amplitudes $n_m^\delta(t)$ to study the importance of the different modes during the modal representation of the neutron flux in the transient. Figures 7, 8, 9 represent the evolution of the amplitudes for the λ, γ and α expansion, respectively. All graphics show that the first coefficient, that corresponds to the first eigenfunction, is the one that contributes in the increasing evolution of the power, since the reactor transient starts from a near critical configuration. This coefficient is equal for all modes since the first eigenfunctions associated to each mode are very similar. Between the subcritical functions, there are meaningful differences. All figures for subcritical harmonics show that the second and third coefficient are out-of-phase. However, these functions have different amplitude depending on the kind of mode and the number of mode. These differences are due to the different shapes that have the 2nd and 3rd eigenfunctions (Figure 5). The n_4^δ and n_5^δ, for all cases, are slightly oscillating, but with values close to zero during all the transient. The next coefficients are not represented since, for all modes, they are close to

zero too.

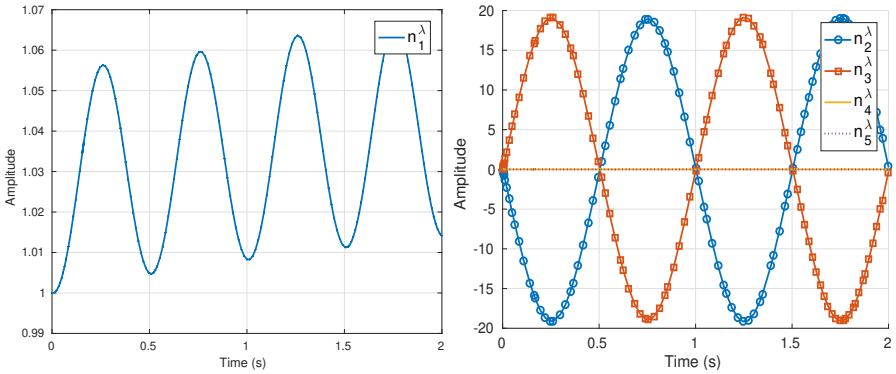

(a) 1st Harmonic (b) 2nd, 3rd, 4th, 5th Harmonics

Figure 7: Evolution of the amplitudes in the λ modal expansion of the Langenbuch reactor.

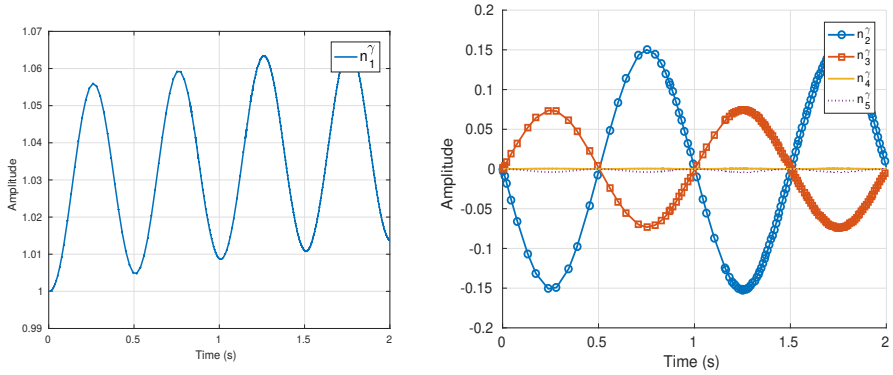

(a) 1st Harmonic (b) 2nd, 3rd, 4th, 5th Harmonics

Figure 8: Evolution of the amplitudes in the γ modal expansion of the Langenbuch reactor.

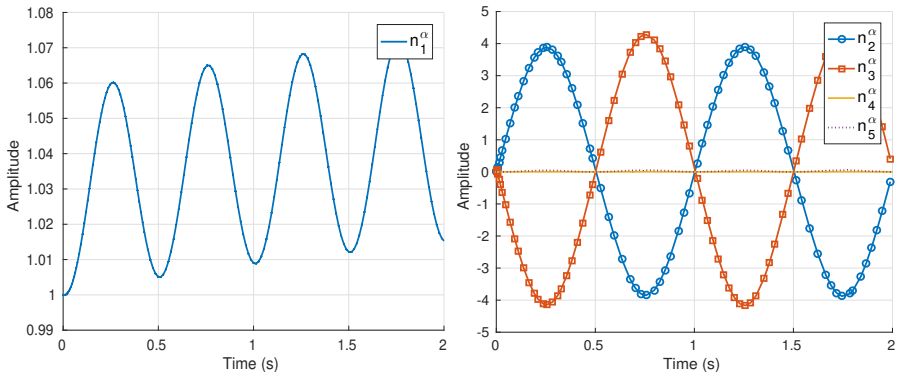

(a) 1st Harmonic (b) 2nd, 3rd, 4th, 5th Harmonics

Figure 9: Evolution of the amplitudes in the α modal expansion of the Langenbuch reactor.

Figure 10 shows the relative power computed with the BKM, and the relative powers computed by using the λ modal expansion for $q = 5$, $q = 10$ and $q = 20$. A similar behaviour is obtained for the γ and α-modes. In this Figure, we can observe that this type of transient needs to be described with a large number of modes because the perturbations are local. This fact is also observed in the evolution of the amplitudes where these values from $q = 3$ are close to zero, and we need a lot of eigenfunctions to obtain accurate approximations for the flux distribution. Regarding the difference with the BKM, we can deduce that the biggest errors are in the relative maximums of the total power, when the $\delta\Sigma_{fg}$ of the perturbations P_1 and P_2 have their relative maximums, and when the spatial distribution of the flux is more different from the spatial distribution of the flux in steady state. These differences increase when the time is larger. Figure 11 displays a comparison between the relative power computed with ten λ, γ and α-modes. In this graphic, we cannot appreciate a large difference between the kind of mode used to compute the total power.

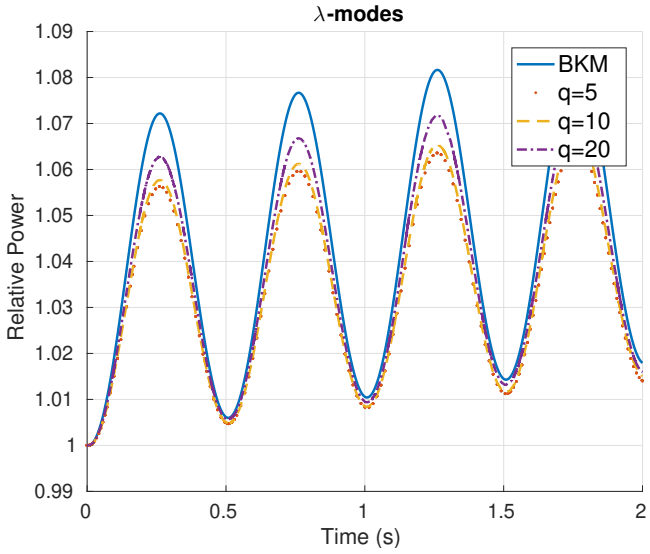

(a) λ

Figure 10: Evolution of the relative power computed with the BKM and the λ modal method of the Langenbuch transient.

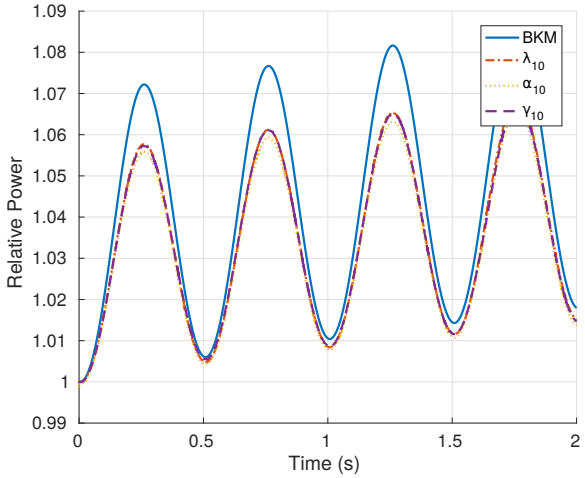

Figure 11: Evolution of the relative power computed with the BKM and the modal method with 10 modes.

However, to study with more detail the errors of the modal methods with respect to the solution obtained with the BKM, we have computed the Mean Power Error (MPE), to quantify the total power errors between the different

modal expansions used, and Radial Power Error (RPE), to observed the spatial distribution of the power error. These errors have been computed for $t = 0.25$ because this is a value where the errors are higher. Table 7 collects the MPEs using $q = 5$ and $q = 10$ modes. It is observed that similar errors are obtained for the different types of modes and that they decrease when the number of eigenvalues is larger. The RPEs have been represented in Figure 12. These graphics show that the errors are placed mainly in the cells near the reflector materials (R) and in the cells that have been perturbed.

Table 7: Mean Power Error (MPE) at $t = 0.25$ of the Langenbuch reactor.

n.eigs (q)	λ-modes	γ-modes	α-modes
5	$1.68e{-}2$	$1.70e{-}2$	$2.89e{-}2$
10	$1.53e{-}2$	$1.55e{-}2$	$1.52e{-}2$

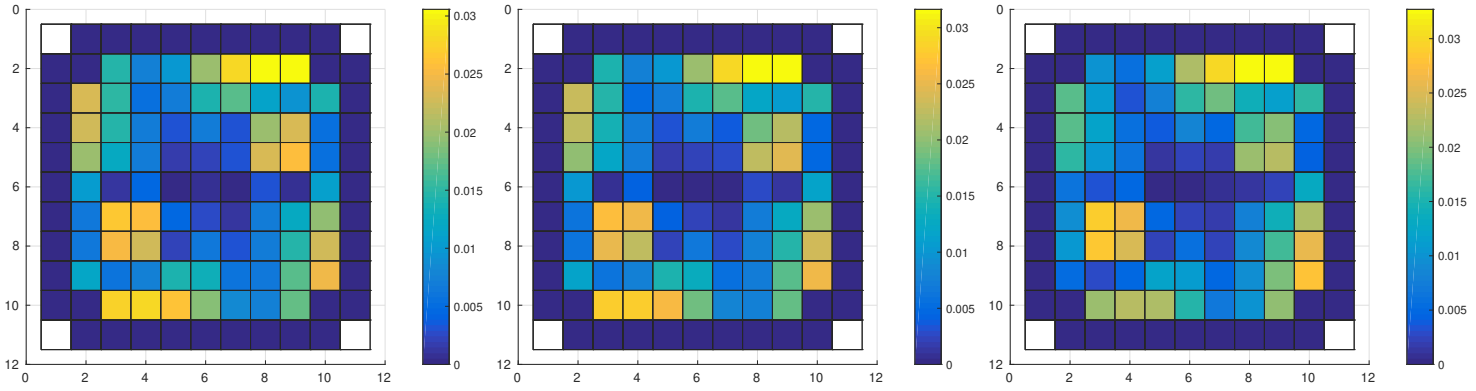

(a) RPE of λ_{10} (b) RPE of γ_{10} (c) RPE of α_{10}

Figure 12: Radial Power Error (RPE) of the Langenbuch transient at $t = 0.25$ with three eigenvalues.

In the following, we analyze the dynamical system of the modal kinetic equations for each one of spatial modes. For that, we have recollected the number of steps used by the backward method of CVODE and the CPU time of the modal expansions to integrate the systems until $t = 2.0$s. Table 8 has the data for $q = 5$ and $q = 10$. Moreover, this Table includes the CPU time to solve the transient problem with the BKM. This Table shows that less stiff systems are obtained by using the α-modes, since we need less time steps to reach $t = 2.0$. However, the modal expansion that computes the solution in less time is the γ modal expansion. Regarding the CPU time obtained with the BKM, one could observed that this methodology takes much more time

to obtain an approximation for the transient than the modal kinetics with the different spatial modes.

Table 8: Number of iterations (n. its) and computational time (s) for the computation of the modal expansion for the Langenbuch reactor.

n.eigs	λ-modes		γ-modes		α-modes		BKM
(q)	n. its	CPU time	n. its	CPU time	n. its	CPU time	CPU time
5	380	699	249	491	136	631	34950
10	199	2426	129	1609	116	1809	

Finally, we choose the frequency of the perturbation of the Equation (36) is set to $\omega = 4Hz$ to analyze the response of the reactor with a frequency away from the plateau region. Figure 13 shows the relative power obtained with the different methods studied in this work for this value of frequency. This Figure shows that the behaviour of the errors obtained with the approximations from the modal kinetics solutions is not dependent on the frequency of the perturbation applied to the time-dependent problem.

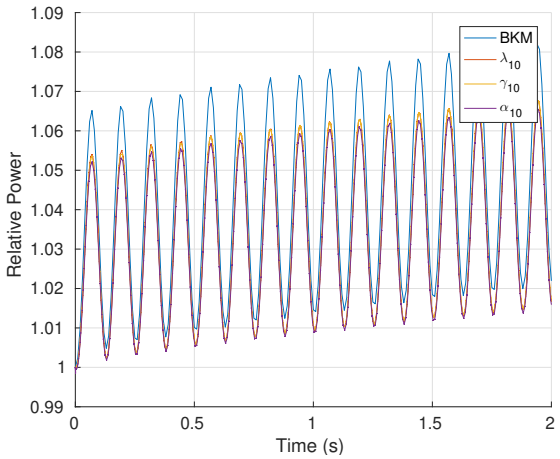

Figure 13: Relative power of the Langenbuch reactor with the perturbation defined in Equation (36) where $\omega = 4Hz$.

5. Conclusions

In this work, we have used the λ, the γ and the α-modes problem to develop different modal kinetic equations to integrate the time dependent neutron diffusion equation. For the spatial discretization of the differential equations, we have used a high order finite element method. The performance of these methods have been analyzed and compared by using two three-dimensional benchmarks. To validate the code implemented, these results have been compared with the

results obtained with the backward differential method (BKM) applied directly to the neutron diffusion equation.

From the obtained results, we can highlight the following conclusions. A modal kinetics with more than one eigenvalue is necessary to describe some types of transient such as the out-of-phase oscillations or the local perturbations. These modal kinetics give more accurate results when the number of eigenvalues considered is larger. The largest differences in the power evolution between the BKM solution and the modal approximations solutions are mainly when the spatial distribution of the power is more different from the power distribution of the reactor in steady state. Henceforth, in future works, to obtain better approximations, the eigenfunctions associated to the modes will be updated along the transient generalizing in this way the quasi-static method. The CPU times obtained with the BKM and the CPU times obtained with the different modal expansions show that the modal methodology is a faster strategy to obtain the solution in the time-dependent problems analyzed.

Regarding the different spatial modes used in the modal expansions, we have not observed meaningful differences between the results in term of the total power evolution of the transients studied. However, there are some differences in the stiffness of the resulting dynamical systems associated with the modal kinetics for each kind of mode. We observed that in the transients analyzed using the α-modes the obtained differential systems are not as stiff as the systems obtained using the λ-modes and γ-modes. Nevertheless, the modal kinetics by using the γ-modes expansion gives the approximations in less time.

In this way we have obtained different modal kinetics equations with different characteristics that can be successfully used to describe reactor transients. In future works, we will extend this study to integrate the neutron diffusion equation with more than two energy groups and to other approximations of the neutron transport equation in order to test benchmark problems such as the C5G7-TD (Boyarinov et al., 2016).

Acknowledgements

This work has been partially supported by Spanish Ministerio de Economía y Competitividad under projects ENE2017-89029-P, MTM2017-85669-P and BES-2015-072901.

References

Abhyankar, S., Brown, J., Constantinescu, E. M., Ghosh, D., Smith, B. F., & Zhang, H. (2018). Petsc/ts: A modern scalable ode/dae solver library. *arXiv preprint arXiv:1806.01437*, .

Adrover, A., Creta, F., Giona, M., & Valorani, M. (2005). Biorthogonalization, geometric invariant properties and rate-based estimate of Lyapunov spectra. *Physics Letters A*, *342*, 421–429.

Akcasuh, Z. (1971). *Mathematical methods in nuclear reactor dynamics*. Elsevier.

Avvakumov, A., Strizhov, V., Vabishchevich, P., & Vasilev, A. (2017a). Modelling dynamic processes in a nuclear reactor by state change modal method. In *Journal of Physics: Conference Series* (p. 012003). IOP Publishing volume 937.

Avvakumov, A. V., Strizhov, V. F., Vabishchevich, P. N., & Vasilev, A. O. (2017b). Spectral properties of dynamic processes in a nuclear reactor. *Annals of Nuclear Energy*, *99*, 68–79.

Avvakumov, A. V., Strizhov, V. F., Vabishchevich, P. N., & Vasilev, A. O. (2018). State change modal method for numerical simulation of dynamic processes in a nuclear reactor. *Progress in Nuclear Energy*, *106*, 240–261.

Balay, S., Abhyankar, S., Adams, M., Brown, J., Brune, P., Buschelman, K., Dalcin, L., Dener, A., Eijkhout, V., Gropp, W. et al. (2018). *PETSc Users Manual: Revision 3.10*. Technical Report Argonne National Lab.(ANL), Argonne, IL (United States).

Bangerth, W., Hartmann, R., & Kanschat, G. (2007). Deal.II – a general purpose object oriented finite element library. *ACM Trans. Math. Softw.*, *33*, 24/1–24/27.

Bernal, Á., Roman, J. E., Miró, R., Ginestar, D., & Verdú, G. (2016). Development of a finite volume inter-cell polynomial expansion method for the neutron diffusion equation. *Journal of Nuclear Science and Technology*, *53*, 1212–1223.

Boyarinov, V., Fomichenko, P., Hou, J., Ivanov, K., Aures, A., Zwermann, W., & Velkov, K. (2016). Deterministic Time-Dependent Neutron Transport Benchmark without Spatial Homogenization (C5G7-TD). *Nuclear Energy Agency Organisation for Economic Co-operation and Development (NEA-OECD)*, .

Carreño, A., Vidal-Ferràndiz, A., Ginestar, D., & Verdú, G. (2017). Spatial modes for the neutron diffusion equation and their computation. *Annals of Nuclear Energy*, *110*, 1010–1022.

Dulla, S., Mund, E. H., & Ravetto, P. (2008). The quasi-static method revisited. *Progress in Nuclear Energy*, *50*, 908–920.

Dulla, S., Ravetto, P., & Saracco, P. (2018). The time eigenvalue spectrum for nuclear reactors in multi-group diffusion theory. *The European Physical Journal Plus*, *133*, 390.

Ginestar, D., Verdú, G., Vidal, V., Bru, R., Marín, J., & Munoz-Cobo, J. (1998). High order backward discretization of the neutron diffusion equation. *Annals of Nuclear Energy*, *25*, 47–64.

Henry, A. (1958). The application of reactor kinetics to the analysis of experiments. *Nuclear Science and Engineering*, *3*, 52–70.

Henry, A. F. (1982). *Nuclear-reactor analysis* volume 4. MIT press Cambridge, Massachusetts.

Hernandez, V., Roman, J. E., & Vidal, V. (2005). SLEPc: A scalable and flexible toolkit for the solution of eigenvalue problems. *ACM Trans. Math. Software*, *31*, 351–362.

Hindmarsh, A. C., Brown, P. N., Grant, K. E., Lee, S. L., Serban, R., Shumaker, D. E., & Woodward, C. S. (2005). SUNDIALS: Suite of nonlinear and differential/algebraic equation solvers. *ACM Transactions on Mathematical Software (TOMS)*, *31*, 363–396.

Lange, C., Hennig, D., Schulze, M., & Hurtado, A. (2014). Complex BWR dynamics from the bifurcation theory point of view. *Annals of Nuclear Energy*, *67*, 91–108.

Langenbuch, S., W.Maurer, & W.Werner (1977). Coarse-mesh flux-expansion method for the analysis of space-time effects in large light water reactor cores. *Nuclear Science and Engineering*, *63*, 437–456.

Lewins, J. (2013). *Nuclear reactor kinetics and control*. Elsevier.

de Lima, Z. R., da Silva, F. C., & Alvim, A. C. M. (2009). A modal multidimensional kinetics method using pseudo-harmonics. *Annals of Nuclear Energy*, *36*, 752–759.

March-Leuba, J., & Blakeman, E. (1991). A mechanism for out-of-phase power instabilities in boiling water reactors. *Nuclear Science and Engineering*, *107*, 173–179.

March-Leuba, J., & Rey, J. (1993). Coupled thermohydraulic-neutronic instabilities in boiling water nuclear reactors: a review of the state of the art. *Nuclear Engineering and Design*, *145*, 97–111.

Miró, R., Ginestar, D., Verdú, G., & Hennig, D. (2002). A nodal modal method for the neutron diffusion equation. Application to BWR instabilities analysis. *Annals of Nuclear Energy*, *29*, 1171–1194.

Modak, R., & Gupta, A. (2007). A scheme for the evaluation of dominant time-eigenvalues of a nuclear reactor. *Annals of Nuclear Energy*, *34*, 213–221.

Ronen, Y., Shvarts, D., & Wagschal, J. (1976). A comparison of some eigenvalues in reactor theory. *Nuclear Science and Engineering*, *60*, 97–101.

Singh, K., Degweker, S., Modak, R., & Singh, K. (2011). Iterative method for obtaining the prompt and delayed alpha-modes of the diffusion equation. *Annals of Nuclear Energy*, *38*, 1996–2004.

Stacey, W. M. (1969). *Space-time nuclear reactor kinetics* volume 5. Academic Press.

Stacey, W. M. (2007). *Nuclear reactor physics*. John Wiley & Sons.

Tommasi, J., Maillot, M., & Rimpault, G. (2016). Calculation of higher-order fluxes in symmetric coresi: Theory. *Nuclear Science and Engineering*, *184*, 174–189.

Velarde, G., Ahnert, C., & Aragones, J. (1978). Analysis of the eigenvalue equations in k, lambda, gamma, and alpha applied to some fast- and thermal-neutron systems. *Nucl. Sci. Eng.*, *66:3*.

Verdú, G., & Ginestar, D. (2014). Modal decomposition method for BWR stability analysis using alpha-modes. *Annals of Nuclear Energy*, *67*, 31–40.

Verdu, G., Ginestar, D., Roman, J., & Vidal, V. (2010). 3D alpha modes of a nuclear power reactor. *Journal of nuclear science and technology*, *47*, 501–514.

Verdú, G., Ginestar, D., Vidal, V., & Miró, R. (1998). Modal decomposition method for BWR stability analysis. *Journal of nuclear science and technology*, *35*, 538–546.

Verdú, G., Ginestar, D., Vidal, V., & Muñoz-Cobo, J. (1994). 3D λ-modes of the neutron-diffusion equation. *Annals of Nuclear Energy*, *21*, 405–421.

Vidal-Ferrandiz, A., Fayez, R., Ginestar, D., & Verdú, G. (2014). Solution of the lambda modes problem of a nuclear power reactor using an *h-p* finite element method. *Annals of Nuclear Energy*, *72*, 338 – 349.

Vidal-Ferràndiz, A., Fayez, R., Ginestar, D., & Verdú, G. (2016). Moving meshes to solve the time-dependent neutron diffusion equation in hexagonal geometry. *Journal of Computational and Applied Mathematics*, *291*, 197–208.

Yamamoto, T., Endo, H., Yokoyama, T., & Kawashima, M. (2010). Implementation of transient neutron transport solver in ASTERIA-FBR. *Proceedings of SNA+ MC*, (pp. 17–21).